ADVANCED FUNCTIONAL MATERIALS
www.afm-journal.de

Skin-like Omnidirectional Stretchable Platform with Negative Poisson's Ratio for Wearable Strain–Pressure Simultaneous Sensor

Min Seong Kim, Yung Lee, Junseong Ahn, Seonggi Kim, Kyungnam Kang, Hyuneui Lim, Byeong-Soo Bae, and Inkyu Park**

Conventional elastomeric polymers used as substrates for wearable platforms have large positive Poisson's ratios (≈0.5) that cause a deformation mismatch with human skin that is multidirectionally elongated under bending of joints. This causes practical problems in elastomer-based wearable devices, such as delamination and detachment, leading to poorly reliable functionality. To overcome this issue, auxetic-structured mechanical reinforcement with glass fibers is applied to the elastomeric film, resulting in a negative Poisson's ratio (NPR), which is a skin-like stretchable substrate (SLSS). Several parameters for determining the materials and geometrical dimensions of the auxetic-structured reinforcing fillers are considered to maximize the NPR. Based on numerical simulation and digital image correlation analysis, the deformation tendencies and strain distribution of the SLSS are investigated and compared with those of the pristine elastomeric substrate. Owing to the strain-localization characteristics, an independent strain-pressure sensing system is fabricated using SLSS with a Ag-based elastomeric ink and a carbon nanotube-based force-sensitive resistor. Finally, it is demonstrated that the SLSS-based sensor platform can be applied as a wearable device to monitor the physical burden on the wrist in real time.

1. Introduction

Over a few decades, conventional electronics based on rigid materials, such as semiconductors, glasses, and composite materials, have been developed and widely utilized in daily life. Nowadays, with broadening application of electronic devices to portable, deformable, and wearable forms, non-rigid material-based electronics with free-form factors such as flexibility, bendability, rollability, and stretchability are required. Currently, wearable electronics are receiving great attention because they enable real-time communication of various information when combined with Internet of Things (IoT). Considering these demands, wearable and stretchable electronic devices have been actively developed and implemented in specific applications such as personal healthcare systems,[1–4] soft robotics,[5–8] virtual reality,[9–11] and human-machine interactions.[12–15]

To realize wearable and stretchable devices, various attempts have been made to integrate conventional rigid electronic devices with stretchable interconnections onto a stretchable substrate, namely rigid-soft hybrid systems, or develop stretchable active/passive electronic components instead of rigid ones. In either approach, a stretchable substrate is an essential element that provides a stable foundation for electronic devices while allowing free deformation. Silicone-based elastomers, such as polydimethylsiloxane (PDMS), have been widely used as stretchable substrates owing to their chemical robustness, biocompatibility, and mechanical flexibility.[16] However, they have a critical limitation in their intrinsic mechanical properties, that is, a high Poisson's ratio (PR) of ≈0.5. In contrast, the human skin can be elongated along multiple directions under a 1-degree of freedom (DOF) bending of the joints.[17] This mismatch of the deformation between the elastomer and skin leads to practical problems of wearable devices, such as user inconvenience, irritation from human-device interfaces, and delamination of devices limits the accuracy of the acquired information.

A few attempts were made to resolve this problem by structuring substrates with a cellular auxetic structure, that is, a

M. S. Kim, J. Ahn, K. Kang, I. Park
Department of Mechanical Engineering
Korea Advanced Institute of Science and Technology (KAIST)
Daejeon 34141, Republic of Korea
E-mail: inkyu@kiast.ac.kr

Y. Lee, B.-S. Bae
Department of Material Science and Engineering
Korea Advanced Institute of Science and Technology (KAIST)
Daejeon 34141, Republic of Korea
E-mail: bsbae@kaist.ac.kr

Y. Lee, B.-S. Bae
Wearable Platform Materials Technology Center (WMC)
Korea Advanced Institute of Science and Technology (KAIST)
Daejeon 34141, Republic of Korea

S. Kim, H. Lim
Nano Nature-inspired Laboratory
Korea Institute of Machinery and Materials (KIMM)
Daejeon 34103, Republic of Korea

The ORCID identification number(s) for the author(s) of this article can be found under https://doi.org/10.1002/adfm.202208792.

DOI: 10.1002/adfm.202208792

mechanical meta-structure showing a negative PR value, that can be stretched omnidirectionally under uniaxial stretching, a deformation tendency similar to that of human skin. Kim et al. introduced an auxetic structured electrode for improved contact with the skin, minimizing delamination and irritation.[18] Lee et al. reported a capacitive stretchable strain sensor based on an elastomer with an auxetic structure.[19] They utilized an auxetic elastomer as a dielectric layer that caused in-plane expansion under stretching, leading to a higher gauge factor of the sensor. They implemented the negative Poisson's ratio (NPR) feature of auxetic structures to not only solve the contact issue but also provide additional functionality. However, these auxetic structure-based components have inherent limitations of structural discontinuity and limited practical areas that are derived from the existence of cut regions, which hinders their universal applicability. Most devices with auxetic structures are implemented as passive electronic elements, such as stretchable electrodes.[20]

To overcome these limitations of the cellular auxetic structures, we modified the elastomeric substrate using an auxetic-patterned glass fabric reinforcement without any discontinuity or cut region on the substrate. In this partially reinforced elastomeric composite, the mechanical deformation was affected by both a stiff glass-fiber-embedded auxetic structure and a soft elastomer matrix. When the disparity in the material properties of the two different domains is substantially large (i.e., the elastic modulus of the auxetic structure inside the elastomer substrate is much higher than that of the elastomer), the substrate expands in the transverse direction of the applied strain by overcoming the contraction originating from the high PR of the soft elastomer matrix, thereby realizing an NPR of the stretchable substrate.[21] A stretchable substrate with extraordinary mechanical characteristics, which has skin-like stretchability, was realized by material hybridization and novel structural design. To achieve this significant NPR characteristic, glass fabrics were utilized as reinforcing materials that satisfied the mechanical robustness and chemical affinity required between the two domains for a minimal interfacial problem.[22,23] The skin-like stretchable substrate (SLSS) was omnidirectionally stretchable regardless of the strain direction owing to the NPR feature. Furthermore, owing to the highly stiffened domains within the auxetic structures, the strain distribution of the SLSS could be locally controlled. This programmable strain localization enables SLSS application as a wearable electronic circuit board with robust electrical interconnections. Unlike conventional stretchable interconnections utilizing stiff islands of serpentine/kirigami, which have direction-dependent characteristics,[24] strain insensitivity was secured under omnidirectional stretching of the substrate. The application of SLSS as a wearable multimodal sensor system that detects strain and pressure independently owing to its novel characteristics in strain distributions was demonstrated.

2. Results and Discussion

The proposed structure and conceptual illustration of the SLSS are presented in **Figure 1**. Conventional elastomeric substrates contract in the transverse direction of stretching by approximately half the applied strain, that is, the PR of the elastomer is ≈0.5 (Figure 1a). In contrast, human skin is elongated multidirectionally under joint bending. This mismatch in deformation causes practical issues such as user inconvenience and irritation. In particular, delamination or detachment phenomena can cause severe problems limiting the reliability and accuracy of the acquired information from wearable devices,

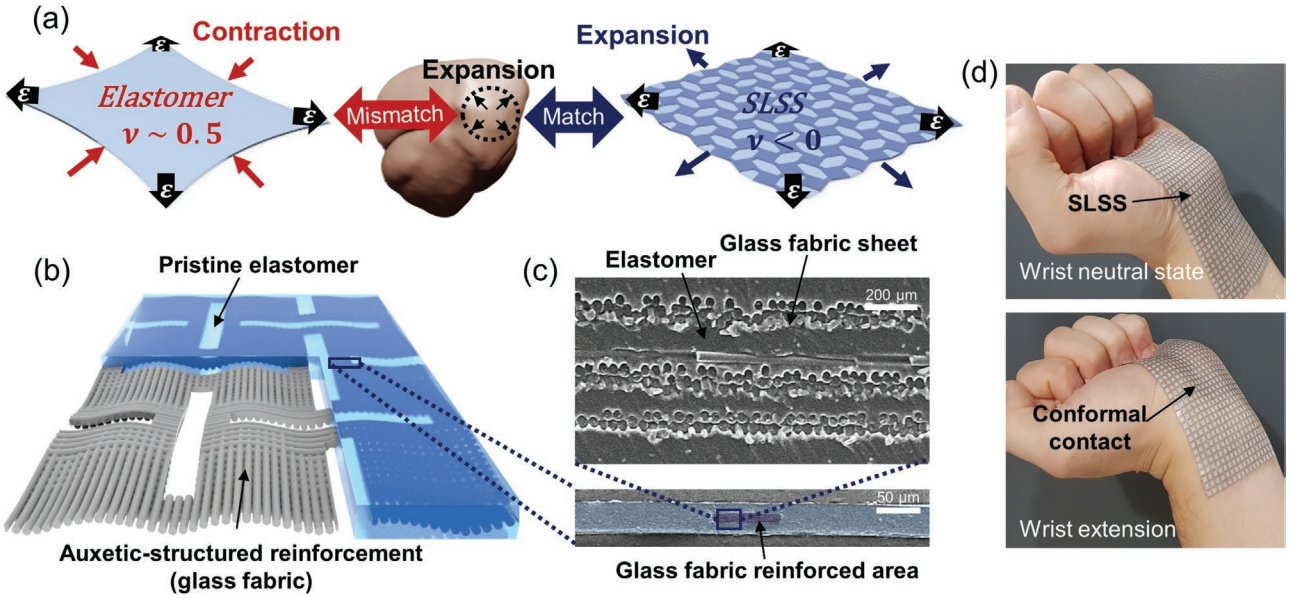

Figure 1. Conceptual schematics and structures of skin-like stretchable substrate (SLSS). a) Deformation tendencies of the bare elastomer, human skin, and the SLSS. b) Structures of the SLSS composed of the auxetic-structured reinforced domain and pristine elastomer domain. c) Microscopic cross-section images of the fabricated SLSS. Scale bars are 20 and 500 μm in upper and lower images, respectively. d) Photographic images showing the conformal contact property of the SLSS to the skin under wrist extension.

even though all the functional elements are trustworthy. To overcome these inevitable problems that may originate from the positive PR of the elastomer, a stretchable substrate with NPR is suggested. The deformation characteristics of the proposed stretchable substrate match well with those of the skin, and this substrate can be called an SLSS.

The SLSS is composed of two different material domains: an auxetic-structured mechanically reinforced domain, and a pristine elastomer domain (Figure 1b). Glass fabric is used as a reinforcing filler owing to its high elastic modulus, good flexibility, and chemical compatibility with silicone-based elastomers (i.e., Si-O-Si bonding).[25,26] In SLSS, the glass fabric is selectively embedded in the elastomer with an auxetic structure, endowing the NPR characteristics.[27] The elastomer matrix impregnates the glass fabric in the reinforcing domain to form a fiber-reinforced plastic (FRP) composite. The remaining elastomer matrix that is not reinforced remains pristine and fills the gaps in the auxetic structure, forming a continuous composite film. The selective reinforcement with glass fabric and the smooth and continuous surface of the fabricated SLSS film was confirmed by scanning electron microscopy (SEM) images of the cross-section of the SLSS (Figure 1c). In the magnified view, the microscale hybridization of the glass fabric and elastomer was confirmed. When applied to the wrist, the SLSS maintains a conformal contact during wrist extension because of its omnidirectional stretchable nature attributable to the NPR characteristics, demonstrating its skin-like stretchable behavior (Figure 1d).

As the two domains have different deformation tendencies under stretching (i.e., auxetic and pristine domains are forced to deform with negative and positive PR, respectively), the SLSS behavior can be affected by several factors, including mechanical properties, geometrical dimensions, and interfacial interactions of the constituent materials. First, we considered the material properties of the two domains, elastomers with and without reinforcement, to determine the deformation of the SLSS. A finite element method (FEM)-based numerical simulation was conducted assuming that the SLSS was formed by two distinct domains with different material models, as shown in Figure S1 (Supporting Information). The pristine cover elastomer was fixed as Ecoflex 00–30 (Smooth On Inc. USA) with the hyperelastic material model, whereas the auxetic reinforced domain was assumed to be a linear elastic material. **Figure 2**a shows the simulation results and the stress distributions of the SLSS with different combinations of mechanical properties. The NPR was revealed when the elastic modulus ratio between the two domains was over ≈5000. The vertical expansion (i.e., the negative Poisson's effect) upon elongation of the SLSS along the horizontal direction is a competition between the expansion force owing to the auxeticity of the reinforced auxetic domain and the contraction force of the pristine elastomer domain. Therefore, the higher the modulus of the auxetic domain and the lower the modulus of the pristine elastomer domain, the greater the decrease in the PR (i.e., the larger the NPR) of the SLSS.

The change in PR with respect to the ratio of the modulus between the two domains is shown in Figure 2b. The method for calculating the PR is explained in Figure S2 (Supporting Information). As the ratio of the modulus is higher, the PR decreases and shows a negative value at the critical point (E_{ratio} ≈500). The results show that the materials comprising the SLSS should have extremely different Young's moduli to ensure an ideal NPR (i.e., theoretical maximum value of the unfilled auxetic structure). In addition, the stretchability of SLSS can be

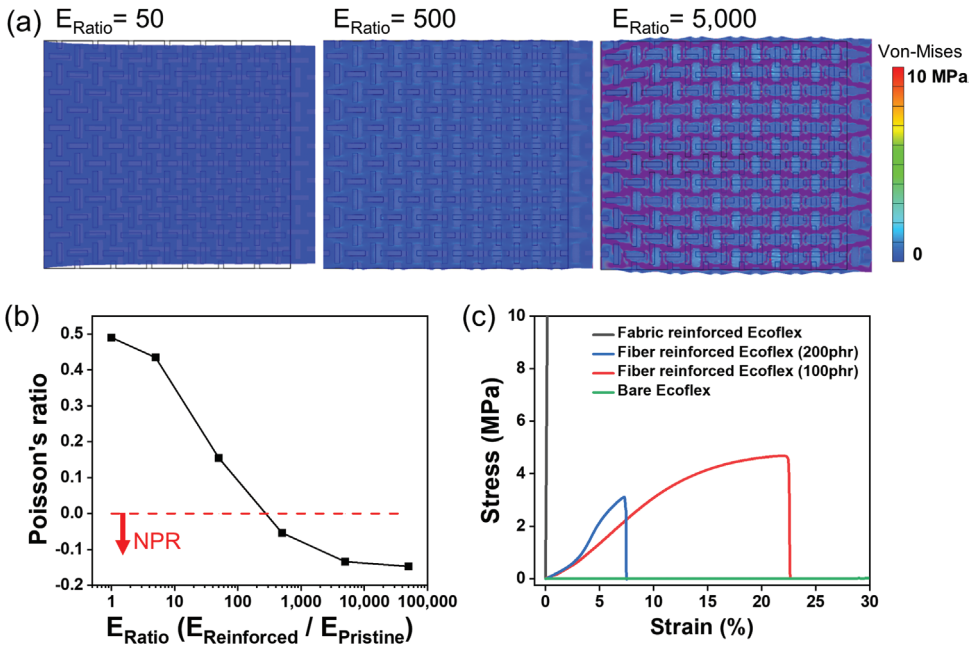

Figure 2. Simulation results showing deformation characteristics of the SLSS and material considerations for the realization of the negative Poisson's ratio (NPR). a) Stress contours and deformation of SLSS, b) calculated PRs under 10% uniaxial strain derived by finite element method (FEM)-based simulation with various ratios in elastic moduli between reinforced and pristine domains of the SLSS, and c) stress–strain curves from tensile test of the polymeric composites with different configuration of reinforcing materials. (phr: parts per hundred rubber)

constrained by the reinforced auxetic structure. Therefore, the material combination of the composites and geometrical design of the auxetic domain should be optimized to achieve not only NPR behavior but also high stretchability in future studies.

To verify the effect of the modulus difference, we fabricated glass fiber-based elastomer films with different types of glass fibers (i.e., discontinuous and continuous fillers) following our previous work.[13,23] Each glass fiber-reinforced elastomer was characterized by tensile testing (Figure 2c). When using discontinuous fibers for reinforcement of the elastomer, the elastic modulus increase was not sufficient to obtain the NPR characteristics. The E_{ratio} (= $E_{reinforced}/E_{pristine}$) values were ≈332 and 535 for 100 and 200 parts per hundred rubber (phr) of the fibers, respectively.[23] In addition, the high glass fiber content (>100 phr) significantly increased the viscosity of the prepolymer mixture, which interfered with the uniform distribution of fibers and processability of SLSS. In the case of the glass fabric-reinforced elastomer, a much higher elastic modulus than that of the bare elastomer was observed (E_{Ratio} > 160 000). Therefore, it was confirmed that the glass fabric reinforcement satisfied the requirement of mechanical properties for the auxetic domain of the SLSS with NPR.

The geometrical dimensions of the SLSS structure, which is another parameter for determining the deformation characteristics, were investigated. **Figure 3**a shows the geometric variables of the auxetic structure of the SLSS. The gray-colored area indicates the rigid part where the glass fabric is embedded, and the gap is filled with the pristine elastomer. The variables *a* and *b* represent the length and width of the rectangular gap, respectively. The adjacent gap was placed at a rotation angle of 90° and spacing h. This alternating pattern was aligned along the *x*- and *y*-axes. The hinge structure, reinforced area between adjacent gaps, bridges two square units and has a length of *b* and width of *h*. For simplification, we set the parameter AR (aspect ratio) as a/b and SR (slit ratio) as a/h.[28] Figure 3b schematically shows the deformed unit cell shape, which explains the principle of the negative Poisson's effect on the auxetic structure. When tension is applied along the *x*-direction, the rigid square is forced to rotate in-plane because the hinges connected to the rigid square are misaligned in the axial direction, leading to overall expansion along both the *x*- and *y*-axes. However, in the case of SLSS, where the gap is filled with an elastomeric material, the omnidirectional expansion of the film is limited by the restoring force of the extended elastomer. Therefore, the negative value of PR is lower than that of a general auxetic structure.[29] To realize the NPR mechanism and investigate the corresponding deformation, SLSS was fabricated using the processes shown in Figure S3 (Supporting Information). Figure 3c shows the DIC results and the calculated PR of the SLSS with various geometrical parameters of the unit cell, which are described in Figure S4 (Supporting Information). The PR of the unit cell was calculated using the following equation:

$$\mathrm{PR} = -\frac{\Delta Y}{\Delta X} \tag{1}$$

where ΔX and ΔY are the displacements on the horizontal and vertical sides of the unit cell, respectively. The structure with a higher SR has a thinner hinge width, which makes the rotation of the rigid square units more facile and induces auxeticity. AR is related to the rigid auxetic domain. A higher AR increases the auxeticity by enlarging the auxetic domain and reducing the PR effect of the pristine elastomers. In addition, the high AR forms a slender gap shape, which accompanies a larger expansion of the gap to the vertical axis. As SR and AR increase, a larger NPR value close to the ideal value of −1 is obtained.[29] However, SLSS with low SR and AR values (AR = 2 and SR<6) shows positive PR because of the influence of the elastomer's

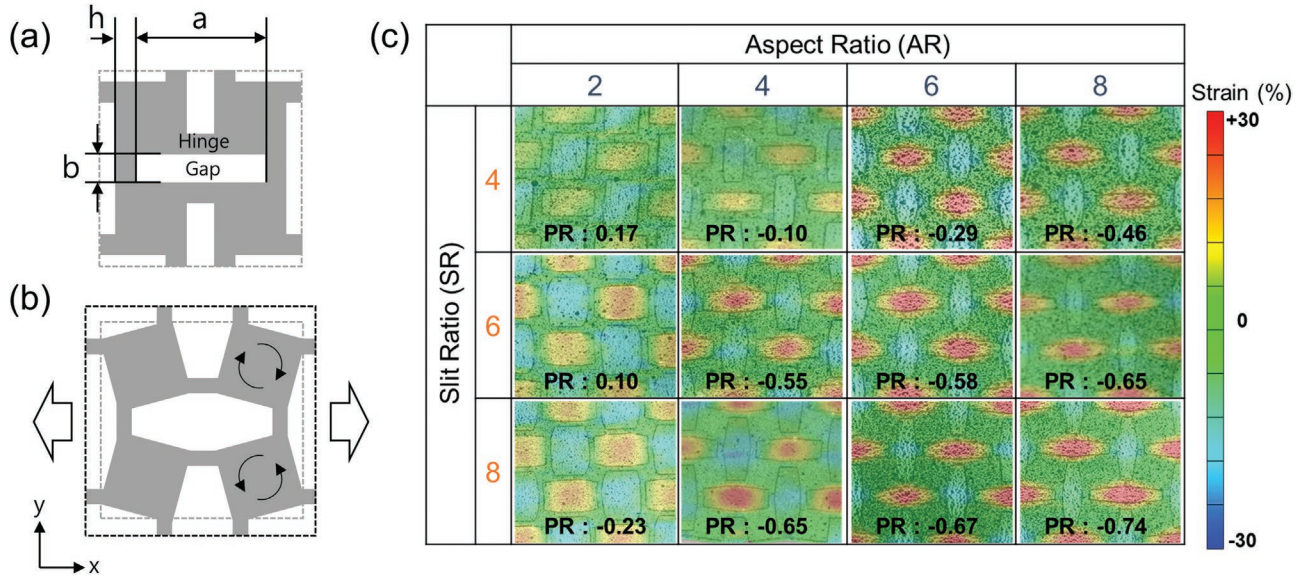

Figure 3. Investigation in a structural design of the SLSS for an analysis of the deformation characteristics. a) Initial and b) deformed shape of the rotating square unit-based auxetic structure with geometrical variables, *a*, *b*, and *h*. c) Local strain distribution measured by digital image correlation (DIC) method and calculated Poisson's ratio (PR) of the SLSS with different geometrical parameters of the embedded auxetic structures. As the aspect ratio (AR) and slit ratio (SR) increase, the PR value becomes more negative.

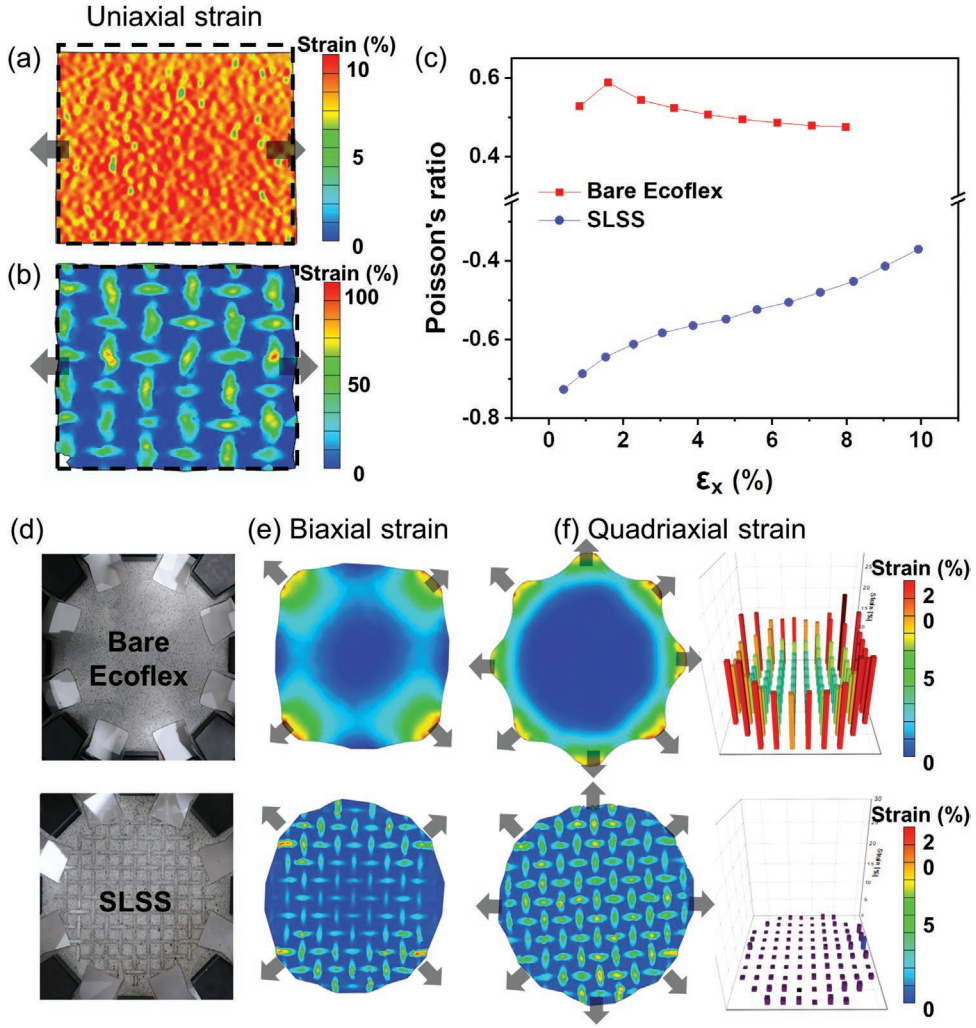

Figure 4. Comparison of deformation characteristics of stretchable substrates with and without auxetic-structured glass fabric. The digital image correlation (DIC) results of a) bare elastomer and b) SLSS showing different strain distributions under uniaxial strain. c) Calculated PR of two different substrates with respect to the applied uniaxial strains along the *x*-axis. d) Setup for multi-axial stretching of the substrate. DIC results of two different stretchable substrates under e) biaxial and f) quadraxial strains. The bar graphs are obtained by calculating the principal strain at identically selective points on the two substrates.

intrinsic mechanical properties even though the auxetic structure is embedded.

A comparison of the deformation of the two stretchable substrates is presented in **Figure 4**. The initial state of each substrate is marked with a black dotted box in the graphical result of the DIC analysis. In Figure 4a, the bare elastomer film shows the well-known deformation characteristics of the elastomer under uniaxial strain, which is a substantial contraction along the transverse direction to the strain. In contrast, the SLSS exhibited a very different tendency. Local strains of the substrate were re-distributed because of the difference in mechanical stiffness of the two domains, leading to an expansion in the stretched as well as the transverse direction. (i.e., The NPR is shown in Figure 4b). Owing to this omnidirectional stretchable characteristic, the SLSS exhibits synclastic bending behavior, which promotes facile adhesion on human joint skin (Figure S5, Supporting Information).[30,31] Also, SLSS showed good reliability under repeated stretching of 1000 cycles with 15% stretch. (Figure S6, Supporting Information) When calculating the PR value of the two different substrates with respect to the applied uniaxial strain, the bare elastomer film showed ≈0.5, as expected, whereas the SLSS exhibited a negative value (Figure 4c). The slight shifting behavior of the PR with respect to the applied strain is a general characteristic of rotating square-shaped auxetic metamaterials.[32,33] This phenomenon occurred because of a nonlinear (i.e., sinusoidal) relationship between the degree of expansion in the axial direction and the rotating angle of the rotating square units.

Moreover, they exhibit different tendencies under multiaxial strain situations. The two substrates were stretched in the biaxial and quadraxial directions using a multiaxial stretching setup (Figure 4d). In case of the bare elastomer, the strain distribution varied with the number of elongated axes, and the local strains were concentrated near the point of action, as analyzed by the DIC results (Figure 4e,f). Therefore, the performances of the devices integrated into the general

elastomer-based wearable platform can be changed or distorted by their positions and direction of deformation. However, the SLSS exhibited a consistent strain distribution regardless of the number and position of strain applications. The spatially uniform strain distribution is caused by the SLSS auxeticity effect, where the rigid auxetic domain expands omnidirectionally owing to external strains. The SLSS expansion was performed predominantly by the auxetic domain, and the soft pristine domain occupying smaller regions in the SLSS underwent strain concentration owing to the high ratio of elastic moduli. Therefore, the auxetic domain regions of the SLSS underwent uniformly low values of strain and were negligibly affected by external strain. The bar graphs obtained by measuring the principal strain applied at the selective points (corresponding to the center of the rotating square unit of SLSS) show varying strain-localization phenomena present within these two substrates. In addition, the lower strain SLSS value indicates its application in strain-sensitive devices. When functional devices are mounted on an SLSS-based wearable platform, their performance and characteristics are reliably secured.

A multimodal wearable sensor system was developed utilizing the deformation characteristics of the SLSS, that is, strain localization. As the strain on the SLSS was locally concentrated or repressed, the amount of strain and stress applied to the integrated functional elements could be controlled by the arrangement of their positions. Based on these characteristics, a sensor system capable of independently sensing pressure and strain can be easily realized. An Ag flake-based elastomeric paste (AgEP) was prepared and used as an element of strain sensor and electrical interconnection. (Details in Experimental Section) For an ultra-sensitive pressure sensor, a carbon nanotube (CNT)-based soft force-sensitive resistor (FSR) was implemented as an ultra-sensitive pressure sensor.[34] This pressure sensor showed highly sensitive electrical responses owing to the gap closing–opening mechanism of the microporous structure of the soft elastomer coated with CNTs.

A photograph of the fabricated sensor system is shown in **Figure 5**a. AgEP was deposited on the hinge of the auxetic region for the electrodes and electrical interconnections. The AgEP was patterned with accurate alignment using a pneumatic-based dispensing system, as shown in Figure S7 (Supporting Information).[35] AgEP has deformation-insensitive intrinsic properties, as shown in Figure S8 (Supporting Information). Moreover, because the stiff auxetic domain of the SLSS underwent negligible strain, the AgEP formed in this area exhibited stable conductance under different stretching directions (0°, 45°, and 90°), as shown in Figure 5b. In contrast, the same material (i.e., AgEP) was used as a strain sensor by adjusting the arrangement of the deposited position and controlling the applied strain. In Figure 5c, the AgEP shows strain-sensitive characteristics when patterned on the gap-filled area of the SLSS, where strains and stresses are highly concentrated. Moreover, the AgEP strain sensor sensitivity could be tuned in the range from 16.7 to 33.3 within a small strain range (<7%) and from 150 to 300 within a large strain range (>7%) by a delicate alignment as a subtle change in position can make a significant difference in the strain concentration, which is proven by a numerical simulation as presented in Figure S9 (Supporting Information). As explained in Figure S8 (Supporting Information), the deformation-insensitive property of the AgEP causes the strain sensor to have pressure-insensitive characteristics, as shown in Figure 5d. Even though a pressure of 1 MPa was applied to the element, relative change in resistance was <0.45%.

For the pressure sensor, the CNT-based FSR was mounted on a stiff rotating unit of an auxetic structure using Ag epoxy. Figure 5e shows that the FSR is highly sensitive (up to 5.45×10^{-3} Pa^{-1}) and exhibits linear responses under pressures ranging from 0 to 50 Pa. Also, $\Delta I/I_0$ of the FSR under pressure was maintained even though the SLSS platform was stretched up to 10% strain. This strain-insensitive characteristic of the integrated FSR is shown in Figure 5f. The FSR initial resistance was negligibly changed (<0.01%) under dynamic uniaxial strains ranging from 0% to 10%. Additionally, the response times of the pressure and strain sensors were measured, as shown in Figure S10 (Supporting Information). In summary, a multimodal sensing system that enables independent detection of strains and pressures was easily realized by utilizing the strain-localization characteristics of the SLSS.

Recently, daily life patterns including frequent use of computers and smartphones have placed a lot of burden on the wrist, which can cause carpal tunnel syndrome (CTS). In particular, prolonged operation of the mouse puts integrated external pressure on the carpal tunnel (CT), worsening the condition.[36] Therefore, to prevent CTS, it is necessary to release the physical burden on the wrist and continuously monitor the mechanical stimuli acting on the CT area. Although there are several ergonomic devices to reduce carpal tunnel pressure (CTP) during mouse operations, such as gel mouse pads and gliding palm supports, a system for real-time monitoring of pressure and strain is required not only for the prevention and recovery but also for the verification of the efficiency of these devices.[37]

Therefore, we have developed a smart wristband that enables monitoring of the strain and pressure applied to the wrist by implementing an SLSS-based sensor platform, as shown in **Figure 6**a. Four CNT-based FSR were mounted on the rotating square unit of the SLSS and AgEP-based strain sensors, and electrodes were formed on the designated regions. Figure S11 (Supporting Information) shows that all sensors (four pressure sensors and one strain sensor) independently functioned under pressure and strain changes. Furthermore, to provide a user-friendly real-time monitoring system, the sensing information from the smart band was transmitted to a smartphone app by Bluetooth communication, which can provide a warning signal when the pressure and strain reach a certain value. The threshold value of the pressure was set to 5 kPa based on the critical pressure value, which potentially impaired the intraneural venular flow.[38] Moreover, the wrist extension induced a tensile strain, and a strain of 10% would result in a similar value of the threshold pressure at the median nerve, therefore, the threshold strain was set as 10%.[39,40]

As a strategy for preventing CTS on mouse operation, a vertical mouse is considered as an alternative to the conventional mouse, which can relieve pressure by avoiding direct contact between the CT and a desk.[37] We operated the conventional and vertical mice while wearing the smart band and measured the pressure and strain simultaneously. During a sequential mouse operation from step i to ix, as shown in Figure 6b, the

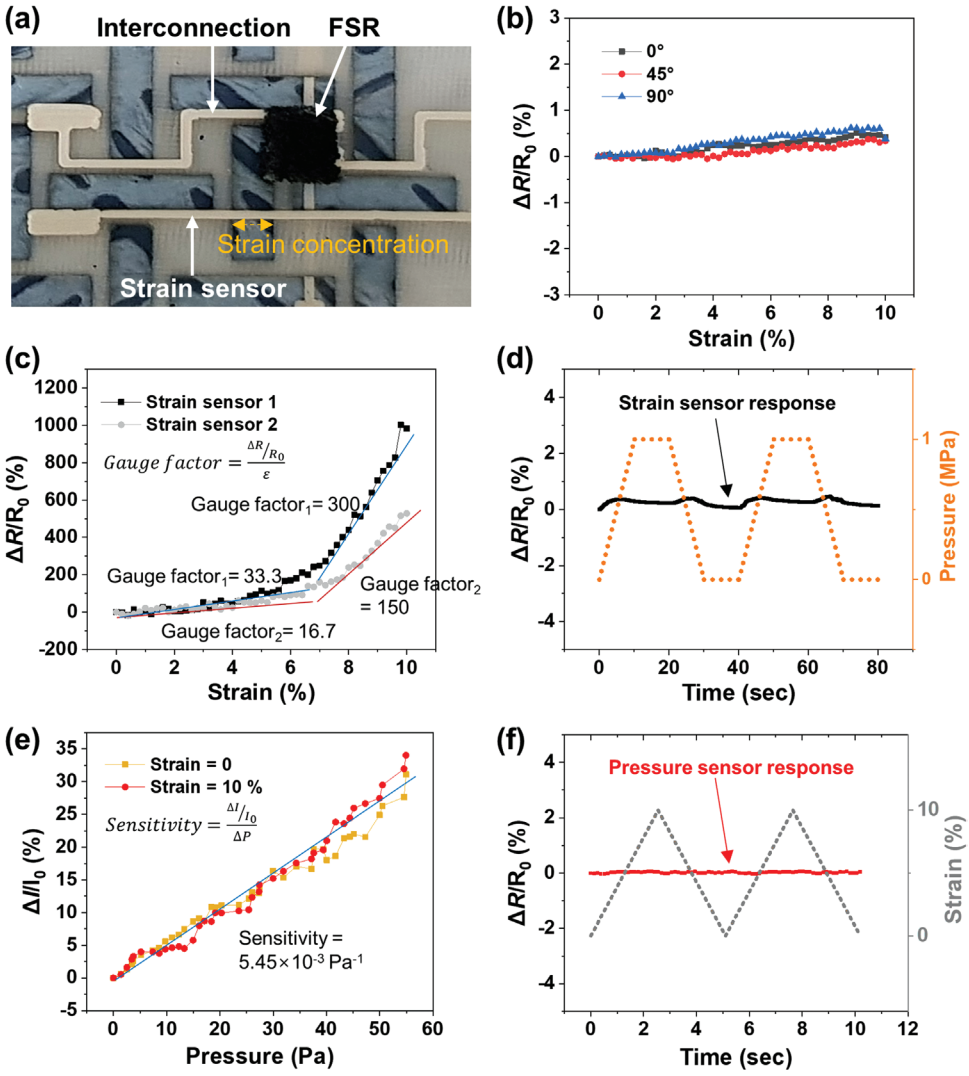

Figure 5. SLSS-based sensor system capable of independent pressure-strain detection. a) A photographic image of the fabricated sensor system composed of the Ag-based elastomeric paste (AgEP) and carbon nanotube (CNT)-based force-sensitive resistor (FSR). b) Electromechanical stability of the AgEP electrodes deposited on the stiff auxetic structure under different angles of stretching. c) Strain-sensitive and d) pressure-insensitive characteristics of the AgEP formed on the filled-gap area. e) Pressure-sensitive and f) strain-insensitive characteristics of the CNT-based FSR mounted on the stiff rotating area of the SLSS.

wrist underwent pressure originating from physical contact with the desk. These external pressures are directly related to stress at the median nerve in the CT, which is the dominant reason for CTS.[36] In contrast, when using the vertical mouse, much smaller pressure and strain were applied under the same operation; thus, the warning signal in the smartphone app rarely appeared, as shown in Figure 6c and Videos S1 and S2 (Supporting Information show the operation of the normal and vertical mouse, respectively, with wireless communication to the smartphone app). Although the use of a vertical mouse can reduce the amount of contact pressure, the claw grip increased the physical burden on the CT area in terms of strain because the extension angle of the wrist became larger than that of the palm grip.[37] This result shows that the SLSS-based wearable device can be utilized in acquisition of real-time and reliable physical sensing data from the human body.

3. Conclusion

In summary, we developed a skin-like stretchable substrate (SLSS) based on an auxetic metamaterial structure and material property engineering. A FEM-based numerical simulation was conducted to verify the proposed deformation mechanism, which has omnidirectional stretchability under unidirectional strain due to the modulus difference between the two domains of the SLSS (i.e., auxetic and pristine domains). SLSS with systematically designed structures and materials were successfully fabricated using solution-based polymer processes and a laser patterning system. The deformation of the SLSS was characterized using the digital image correlation (DIC) method and analyzed by comparing it to the simulation results. Based on the SLSS properties, a wearable sensor platform that can independently measure strain and pressure is realized. Finally, we

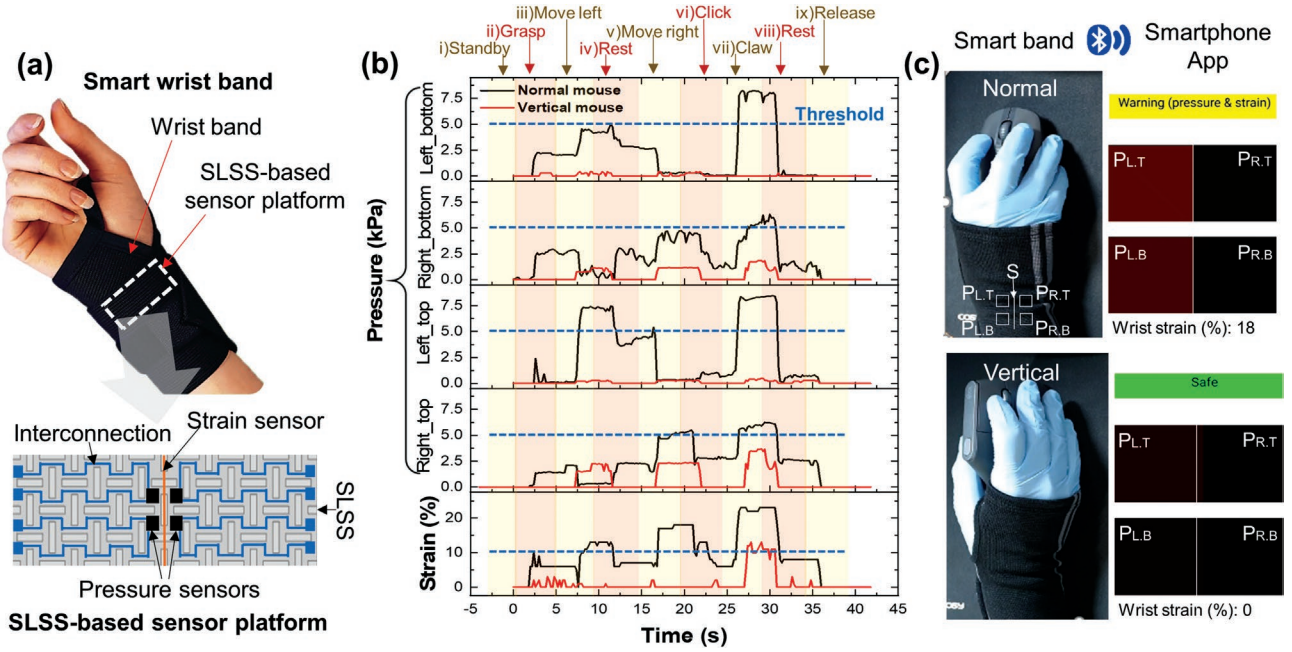

Figure 6. Application to smart wristband to prevent carpal tunnel syndrome (CTS) on operating the mouse. a) Schematic structure of the smart band implemented by the SLSS-based sensor platform to the commercial wristband. b) Responses from the pressure and strain sensors during a sequential operation of the conventional and vertical mice. Blue-dotted lines in the graphs represent the threshold values for the warning signal. c) Photographic images of the mouse operation and corresponding feedback from the smartphone app to display a warning alarm via Bluetooth communication.

demonstrated that the SLSS-based sensor system can be utilized as a smart band for the prevention and recovery of CTS through real-time monitoring of the physical burden on the wrist. This research can have a potential impact on wearable electronics by introducing a universal stretchable substrate that can provide reliable and accurate information from human motion leading to the realization of real-time healthcare, virtual reality (VR), and human-machine interaction for the next-generation industry. For example, monitoring of the applied pressure (up to 3 MPa) and body strain (up to 40%) is helpful in preventing injuries and correcting posture during weight training.[41,42] As conventional devices focus on the monitoring of individual pressure or strain with different systems, it would be advantageous to apply a monolithic wearable platform integrated with pressure and strain sensors using our technology. We expect that our platform can be further applied to next-generation wearable devices by integrating it with recently reported high-performance sensors.

4. Experimental Section

Fabrication of Glass Fiber/Fabric-Reinforced Elastomer: A silicone-based elastomer (Ecoflex 00–30, Smooth-on, USA) was used as the elastomeric matrix for the SLSS. To characterize the material properties of the reinforced domain of the SLSS for the numerical simulation, a glass fiber/fabric-reinforced elastomer was fabricated. For the discontinuous fiber reinforcement of the elastomer, milled glass fibers (FIBERMAN Co., Korea) with average lengths and diameters of 300 and 13.5 µm, respectively, were used.[13] For the glass-fabric-reinforced elastomer, a 25 µm thick woven glass fabric (Nitto Boseki, Japan) was used. Prior to the fabrication of the composite film, O_2 plasma treatment was performed on the glass fabric to generate a hydroxyl group that could form chemical cross-linking with the silicone-based elastomer. Several layers of glass fabric were impregnated into the elastomer and then formed as a film using a vacuum-bag pressing process.[43] After curing the film, an auxetic pattern was formed using a CO_2 laser cutter (LP-400 Series, Panasonic, Japan). The auxetic-shaped glass fabric-reinforced elastomer was impregnated into the elastomer prepolymer and cured again to fill the gap.

Mechanical Characterization of the Reinforced Elastomer: The fiber-reinforced elastomer was prepared by molding a mixture of glass fibers and elastomer prepolymer. A mold with the standard shape for tensile testing of rubber (ASTM D-412) was fabricated using a stereolithography (SL)-type 3D printer (Object 30 Pro, Stratasys Ltd., USA). For an easy detachment of the composite, the 3D printed mold was hydrophobically treated using a perfluoropolyether (PFPE) solution. In contrast, the fabric-reinforced Ecoflex was structured as the standard auxetic shape by the laser cutting system (LP-400 Series, Panasonic, Japan). The prepared specimen was loaded onto a universal testing machine (AGS-X Series, Shimadzu Co., Japan) with pneumatic-based grips for tensile testing. A displacement-controlled mode was used during the test, and the stretching speed was set to 50 mm min^{-1}.

Strain Mapping Through Digital Image Correlation: Digital image correlation (DIC) analysis was used to investigate the strain distribution on the stretchable substrates. For the DIC analysis, speckle patterning on the specimens was conducted using spray paint (Rust-Oleum, USA). Digital images were taken using a digital camera (800D, Canon, Japan). For strain mapping, the images were processed using DIC software (ARAMIS Professional, GOM GmbH, Germany).

Fabrication of the SLSS-based Multimodal Sensor System: Ag-based elastomeric paste (AgEP) was prepared by incorporating 700 phr of Ag flakes (DSF-500MWZ-S, Daejoo Electronic Materials Co., Korea) in a commercial elastomeric polymer (Ecoflex 00–30, Smooth On Inc., USA). For uniform dispersion and electrical performance optimization, a chemical additive (4-methyl-2-pentanone, Daejung Chemicals & Metals Co., Korea) was added at a concentration of 50 phr. The mixture was gently blended with a spatula and then uniformly mixed using an overhead stirrer (HS-T, Daihan Scientific Co., Korea) at 300 rpm for 1 h. The AgEP was contained in a pneumatic-based dispensing system

(information) and patterned along a programmed trajectory. The moving speed of the nozzle was 250 mm min^{-1}, and the air pressure for dispensing was 50 kPa, which were the optimized conditions for precise patterning at the designated position. The AgEP was utilized as both an electrode and a strain sensor by adjusting its patterned positions. A CNT-based force-sensitive resistor (FSR) was mounted on the AgEP electrodes to form a pressure sensor using a commercial Ag epoxy as a conductive adhesive.

Electromechanical Testing of Sensing Elements and Electrodes: A linear-guided moving stage, a universal testing machine, and electronic measuring equipment were used to test the electromechanical responses of the strain sensors, electrodes, and FSRs formed on the SLSS. To characterize the strain-related responses, the SLSS-based integrated system was loaded on the linear stage, and the corresponding resistance of the elements was measured using a source meter (2400 Series, Keithley Instrument, USA) while the stage was actuated. Similarly, when investigating the pressure-related responses, the SLSS was placed on a universal testing machine (AGS-X Series, Shimadzu Co., Japan) and the element was pressed using a customized ceramic tip mounted on the machine. As the tip size was specified, the pressure value was calculated using the measured forces.

Smart Wristband Application: This experiment was approved by the institutional review board (IRB) of Korea Advanced Institute of Science and Technology (KAIST) (IRB No. KH2021-151). All participants provided written, informed consent to participate in this study. To fabricate a smart wristband, four FSRs and one strain sensor were integrated into the stretchable platform, and a system for measuring the sensor array signal was developed. The measurement system was constructed using an Arduino nano33 IoT device and a mobile phone app designed using MIT App Inventor 2 (Google, USA). Then, the stretchable platform with the sensor array and measuring system was integrated into a commercial wristband. During the experiments, a mobile phone received strain/pressure signals from an Arduino device using the Bluetooth Low Energy (BLE 4.0) communication protocol. In these experiments, all FSRs were calibrated using a tensile tester (AGS-X, Shimadzu, Japan) and the strain sensor was calibrated using a customized linear stage.

Supporting Information

Supporting Information is available from the Wiley Online Library or from the author.

Acknowledgements

This work was supported by the Wearable Platform Materials Technology Center (WMC) funded by the National Research Foundation of Korea (NRF) grant from the Korean Government (MSIT) (NRF-2022R1A5A6000846 and 2021M3D1A2049869). This work was also supported by the National Research Foundation of Korea (NRF) grant funded by the Korean government (MSIT) (No.2021R1A2C3008742). This research was also supported by Ministry of Culture, Sports and Tourism and Korea Creative Content Agency (Project Number: R2021040018).

Conflict of Interest

The authors declare no conflict of interest.

Author Contributions

M. S. K., Y. L., and J. A. contributed equally to this work. The manuscript was written through the contributions of all authors. All the authors approved the final version of the manuscript.

Data Availability Statement

Research data are not shared.

Keywords

auxetic structures, negative Poisson's ratio, pressure sensors, strain sensors, stretchable platforms, wearable electronics

Received: July 31, 2022
Revised: October 18, 2022
Published online: November 14, 2022

[1] Y. S. Oh, J. H. Kim, Z. Xie, S. Cho, H. Han, S. W. Jeon, M. Park, M. Namkoong, R. Avila, Z. Song, S. U. Lee, K. Ko, J. Lee, J. S. Lee, W. G. Min, B. J. Lee, M. Choi, H. U. Chung, J. Kim, M. Han, J. Koo, Y. S. Choi, S. S. Kwak, S. B. Kim, J. Kim, J. Choi, C. M. Kang, J. U. Kim, K. Kwon, S. M. Won, et al., *Nat. Commun.* **2021**, *12*, 5008.
[2] Y. Jeong, J. Gu, J. Byun, J. Ahn, J. Byun, K. Kim, J. Park, J. Ko, J. ho Jeong, M. Amjadi, I. Park, *Adv. Healthcare Mater.* **2021**, *10*, 2170042.
[3] K. Kim, J. Choi, Y. Jeong, I. Cho, M. Kim, S. Kim, Y. Oh, I. Park, *Adv. Healthcare Mater.* **2019**, *8*, 1900978.
[4] W. Lee, S. H. Jeong, Y. W. Lim, H. Lee, J. Kang, H. Lee, I. Lee, H. S. Han, S. Kobayashi, M. Tanaka, B. S. Bae, *Sci. Adv.* **2021**, *7*, abi6290.
[5] C. Majidi, *Soft Robot* **2014**, *1*, 5.
[6] C. Laschi, B. Mazzolai, M. Cianchetti, *Sci Robot* **2016**, *1*, aah3690.
[7] S. I. Rich, R. J. Wood, C. Majidi, *Nat. Electron.* **2018**, *1*, 102.
[8] J. Ahn, Y. Jeong, Z. J. Zhao, S. Hwang, K. Kim, J. Ko, S. Jeon, J. Park, H. Kang, J. H. Jeong, I. Park, *Adv. Mater. Technol.* **2020**, *5*, 2070013.
[9] M. Amjadi, A. Pichitpajongkit, S. Lee, S. Ryu, I. Park, *ACS Nano* **2014**, *8*, 5154.
[10] S. Mishra, Y. S. Kim, J. Intarasirisawat, Y. T. Kwon, Y. Lee, M. Mahmood, H. R. Lim, R. Herbert, K. J. Yu, C. S. Ang, W. H. Yeo, *Sci. Adv.* **2020**, *6*, aay1729.
[11] O. Gul, K. Kim, J. Gu, J. Choi, D. del Orbe Henriquez, J. Ahn, I. Park, *ACS Appl Electron Mater* **2021**, *3*, 4027.
[12] M. S. Kim, K. Kim, D. Kwon, S. Kim, J. Gu, Y. S. Oh, I. Park, *Langmuir* **2020**, *36*, 8939.
[13] M. S. Kim, S. Kim, J. Choi, S. Kim, C. Han, Y. Lee, Y. Jung, J. Park, S. Oh, B. S. Bae, H. Lim, I. Park, *ACS Appl. Mater. Interfaces* **2022**, *14*, 1826.
[14] J. Choi, D. Kwon, B. Kim, K. Kang, J. Gu, J. Jo, K. Na, J. Ahn, D. del Orbe, K. Kim, J. Park, J. Shim, J. Y. Lee, I. Park, *Nano Energy* **2020**, *74*, 104749.
[15] H. E. Lee, D. Lee, T. I. Lee, J. Jang, J. Jang, Y. W. Lim, J. H. Shin, S. M. Kang, G. M. Choi, D. J. Joe, J. H. Kim, S. H. Lee, S. H. Park, C. B. Park, T. S. Kim, K. J. Lee, B. S. Bae, *ACS Appl. Mater. Interfaces* **2022**, *14*, 28258.
[16] J. Kang, Y. W. Lim, I. Lee, S. Kim, K. Y. Kim, W. Lee, B. S. Bae, *ACS Appl. Mater. Interfaces* **2022**, *14*, 24840.
[17] A. M. Wessendorf, D. J. Newman, *IEEE Trans. Biomed. Eng.* **2012**, *59*, 3432.
[18] H. W. Kim, T. Y. Kim, H. K. Park, I. You, J. Kwak, J. C. Kim, H. Hwang, H. S. Kim, U. Jeong, *ACS Appl. Mater. Interfaces* **2018**, *10*, 40141.
[19] Y. J. Lee, S. M. Lim, S. M. Yi, J. H. Lee, S. Gyu Kang, G. M. Choi, H. N. Han, J. Y. Sun, I. S. Choi, Y. C. Joo, *Extreme Mech Lett* **2019**, *31*, 100516.
[20] K. I. Jang, H. U. Chung, S. Xu, C. H. Lee, H. Luan, J. Jeong, H. Cheng, G. T. Kim, S. Y. Han, J. W. Lee, J. Kim, M. Cho, F. Miao, Y. Yang, H. N. Jung, M. Flavin, H. Liu, G. W. Kong, K. J. Yu, S. il

Rhee, J. Chung, B. Kim, J. W. Kwak, M. H. Yun, J. Y. Kim, Y. M. Song, U. Paik, Y. Zhang, Y. Huang, J. A. Rogers, *Nat. Commun.* **2015**, *6*, 6566.

[21] B.-S. Bae, Y. Lee, *Omni-Directional Stretchable Fiber Reinforced Composite Film and Manufacturing Method Thereof*, Republic of Korea, **2022**.

[22] J. Beter, B. Maroh, B. Schrittesser, I. Mühlbacher, T. Griesser, S. Schlögl, P. F. Fuchs, G. Pinter, *Polymers (Basel)* **2021**, *13*, 36.

[23] J. Jang, H. G. Im, D. S. Lim, B. S. Bae, *Compos. Sci. Technol.* **2021**, *201*, 108527.

[24] J. Lyu, M. D. Hammig, L. Liu, L. Xu, H. Chi, C. Uher, T. Li, N. A. Kotov, *Appl. Phys. Lett.* **2017**, *111*, 161901.

[25] M. S. Kim, S. Kim, J. Choi, S. Kim, C. Han, Y. Lee, Y. Jung, J. Park, S. Oh, B. S. Bae, H. Lim, I. Park, *ACS Appl. Mater. Interfaces* **2022**, *14*, 1826.

[26] K. Chansomwong, Y. H. Kim, H. Lee, B.-S. Bae, *J Solgel. Sci. Technol.* **2020**, *95*, 447.

[27] L. Mizzi, K. M. Azzopardi, D. Attard, J. N. Grima, R. Gatt, *Physica Status Solidi – Rapid Research Letters* **2015**, *9*, 425.

[28] A. Slann, W. White, F. Scarpa, K. Boba, I. Farrow, *Phys Status Solidi B Basic Res* **2015**, *252*, 1533.

[29] J. N. Grima, P. S. Farrugia, C. Caruana, R. Gatt, D. Attard, *J. Mater. Sci.* **2008**, *43*, 5962.

[30] R. Lakes, *Science* **1987**, *235*, 1038.

[31] A. Alderson, K. L. Alderson, G. Chirima, N. Ravirala, K. M. Zied, *Comp. Sci. Technol.* **2010**, *70*, 1034.

[32] J. N. Grima, K. E. Evans, *J. Mater. Sci. Lett.* **2000**, *19*, 1563.

[33] P. D. Dubrovski, N. Novak, M. Borovinšek, M. Vesenjak, Z. Ren, *Polymers (Basel)* **2019**, *14*, 571.

[34] S. Kim, S. Oh, Y. Jung, H. Moon, H. Lim, *ACS Omega* **2018**, *3*, 1110.

[35] N. Vignais, J. Weresch, P. J. Keir, *Crit Rev Biomed Eng* **2016**, *44*, 397.

[36] S. Kim, M. Amjadi, T. I. Lee, Y. Jeong, D. Kwon, M. S. Kim, K. Kim, T. S. Kim, Y. S. Oh, I. Park, *ACS Appl. Mater. Interfaces* **2019**, *11*, 23639.

[37] A. B. Schmid, P. A. Kubler, V. Johnston, M. W. Coppieters, *Appl Ergon* **2015**, *47*, 151.

[38] G. Lundborg, R. H. Gelberman, M. Minteer-Convery, Y. F. Lee, A. R. Hargens, *Journal of Hand Surgery* **1982**, *7*, 252.

[39] T. W. Wright, F. Glowczewskie, D. Wheeler, G. Miller, D. Cowin, *J Bone Joint Surg Am* **1996**, *78*, 1897.

[40] P. J. Keir, J. M. Bach, M. Hudes, D. M. Rempel, *Hum Factors* **2007**, *49*, 88.

[41] J. Gu, J. Ahn, J. Jung, S. Cho, J. Choi, Y. Jeong, J. Park, S. Hwang, I. Cho, J. Ko, J. H. Ha, Z. J. Zhao, S. Jeon, S. Ryu, J. H. Jeong, I. Park, *Nano Energy* **2021**, *89*, 106447.

[42] Y. Jeong, J. Gu, J. Byun, J. Ahn, J. Byun, K. Kim, J. Park, J. Ko, J. ho Jeong, M. Amjadi, I. Park, *Adv. Healthcare Mater.* **2021**, *10*, 2001461.

[43] J. Jin, J. H. Ko, S. Yang, B. S. Bae, *Adv. Mater.* **2010**, *22*, 4510.